# IDETC2024-143351

#### DESIGN OF ROTATING NONLINEAR PENDULUM VIBRATION ABSORBERS FOR ELECTRIFIED MACHINERY

Pratibha Singh<sup>†,\*</sup>, Ryan Monroe<sup>†</sup>, Bruce Geist,

Department of Mechanical Engineering, Oakland University, Rochester, MI, USA

# **ABSTRACT**

Centrifugal pendulum vibration absorbers (CPVAs) are passive devices and a proven technology for reducing torsional vibrations in rotating systems, including helicopter rotors and crankshafts of internal combustion engines. CPVAs consist of pendulums mounted on a rotor, driven by system rotation, and tuned to counteract engine-order fluctuating torques acting on the rotor, thereby smoothing vibrations. In this study, a unifilar CPVA configuration is proposed to address torsional vibrations in electric machines (EMs). A principal challenge in this application is the high-orders of torsional vibration inherent in current EM operation. As order increases, the path radius of curvature that the absorber mass is required to follow (for proper tuning) diminishes, which presents machining challenges. A dynamic model for a unifilar CPVA is developed and then linearized to compute the tuning orders of the system. A quadratic formula is derived whose roots govern the two natural orders of the system and initial results show a desirable large separation between these orders in a prototype design. The developed model will facilitate future simulation studies of the system forced vibration response to characterize the stability and vibration control performance of this design.

Keywords: Vibration, Unifilar configuration, Bifilar configuration, Double Pendulum, Electric motors, Tuning order

# 1. INTRODUCTION

Recognizing the risks that climate change poses to communities and ecosystems around the world, the international community has adopted the Paris Agreement with the goal to limit global warming to well below 2°C compared to pre-industrial temperatures [1]. Electric vehicles (EV) are a critical technology to decarbonize road transport. There is transformation in vehicle engineering as drivelines and powertrain electrify. Electric motors are at the heart of an EV propulsion system and torsional vibrations in electric motors produces problematic vibration and

Documentation for asmeconf.cls: Version 1.36, June 3, 2025.

audible noise. Due to the increasing price volatility and supply chain issues of rare earth metals, there is a growing need for rare-earth-free motors. A particularly promising Electric motor (EM), the switched reluctance machine (SRM), is able to achieve high levels of efficiency without relying on rare earth metals. This characteristic not only makes it environmentally friendly but also reduces dependency on scarce resources. Despite these advantages, SRMs have encountered limited adoption primarily because of its tendency to experience torsional vibrations, leading to undesirable noise emissions during operation. This has hindered broader acceptance and utilization of SRMs across various sectors [2].

Centrifugal pendulum vibration absorbers (CPVAs) have become an important technology for correcting torsional vibrations in the latest generation of fuel-efficient internal combustion engines (ICEs) and hybrid electric vehicles [3]. Similar to ICEs, EMs generate torque fluctuations at a frequency that is a specific multiple of average rotation speed or order. When properly tuned to a given order, CPVAs can smooth torsional vibrations across all operating speeds. Because they are tuned to correct a specific order of vibtration, CPVAs are potentially more effective than a frequency-tuned device that typically offers correction at fixed frquency, and hence within a narrow window of engine speeds. Just as in ICEs, CPVAs may provide a way to address problematic torsional excitation orders generated by EMs. Because torsional vibration is a major issue for SRMs in particular, coupling CPVA and SRM technology could enable a wider adoption of SRMs, which have currently been relegated to noise-insensitive applica-

A principal challenge with implementing CPVAs in EMs is that they must be able to address the high-orders of vibration inherent in current EM operation. EM vibration orders are significantly higher than the typical combustion-generated orders present in most ICE applications (typically 2, 3, or 4 depending on the number of engine cylinders). Since the absorber mass path radius of curvature is proportional to the inverse of the tuning order squared, the machining precision required to manufacture the small path curvatures in high-order pendulum designs can quickly

 $<sup>^{\</sup>dagger}$ Joint first authors

<sup>\*</sup>Corresponding author

become challenging if not all-together infeasible. Implementing a high-order design requires careful consideration of the CPVA suspension mechanism, which prescribes the relative motion between the absorber and the host rotor. Many designs have been developed to suspend the pendulum absorber mass to the rotor of interest, including a simple pendulum, a roll-form absorber, a unifilar absorber (single-point suspension) and most commonly a bifilar absorber (two-point suspension) [4]. These suspensions have been known for decades and the configurations shown in Figure 1 are most commonly implemented in practice [5] [6].

As shown in Figure 1 (a), the roller-in-slot configuration has the simplest construction of the three, where the roller acts as the pendulum. Since torsional vibration reduction is proportional to the amount of absorber mass present, meeting vibration reduction targets can lead to a larger roller radius. However, more importantly, roller slip is a prominent possibility in a roller-in-slot CPVA, because the roller is not controlled by a diametrical pinch of any kind. Roller slip may interfere with CPVA dynamics and impair correction performance.

Shown in Figure 1 (b) is a bifilar CPVA, which is the most common suspension used in practice, especially in ICE applications as it can accommodate non-circular paths. Noncircular, Epcycloidal paths have performance advantages when considering the nonlinear softening characteristics present in circular path design [7]. However, with the already stringent tolerances on the path radius of curvature in a high-order design, non-circular path curvatures would require even further precision which is impractical considering the torsional orders present in current EMs.

As shown in Figure 1 (c), the unifilar-type absorber is mechanically simpler than the bifilar suspension as the component parts can all be produced by simple boring and turning operations [6], and like the roller-in-slot design, is more practical for machining path curvatures for high-order designs. Unlike the other two designs shown in Figure 1 (a) and (b), a unifilar CPVA is a double pendulum and is commonly referred to as centrifugal double pendulum vibration absorber (CDPVA), since it has two degrees-of-freedom (DOFs) and therefore two tuning orders. Unlike the bifilar suspension, a unifilar pendulum can rotate relative to its unison motion with the roller. Being able to tune a single CPVA to two orders has been exploited by previous researchers for specific multi-order applications including helicopter rotor hub vibration [8] and ICE cylinder deactivation [9]. The study by Manchi et al. [9] used a compound pendulum-type CDPVA, which suspends the rotating pendulum inertia from a pivot point attached to the rotor. Another recent study by Mahe et al. [10], used a CDPVA type similar to the rolling cylinder and ring configuration shown in Figure 1 (c), except that the pendulum mass (cylinder) is suspended on the inside of a hollow roller ring that rolls within the cut-out on the rotor. Similar to our study here, the Mahe et al. [10] design was for an EM application, which involved tuning one of the two resonances to the single-order of excitation. Despite the two orders involved which can further complicate the design in a single-order application, the linear tuning appeared feasible due to the large separation between the resulting tuning orders.

In this work, we develop a dynamic model for the unifilar configuration shown in Figure 1 (c), which suspends a large

rolling pendulum ring from a small roller pin. Unique to our model development, we specifically enforce a symmetry in the radius of the cutout on the rotor to be equivalent to that of the inner pendulum ring, which under strong centrifugal loading results in a diametrical pinch on both sides of the roller (between the rotor and the pendulum) that tends to limit the propensity of the roller to slip during operation [11]. The equations of motion (EOM) for this unifilar CPVA configuration are developed and then subsequently linearized to investigate the linear tuning orders of this system. From the linear EOM, a quadratic formula is derived whose roots yield the two system tuning orders. We further show that this configuration is capable of producing CPVA designs with a desirable large separation between the tuning orders. These developed EOM will provide a basis for future simulation studies that will investigate the forced vibration response of the system including the stability of the absorber response and its resulting performance at reducing the torsional fluctuations of the rotor. Although circular paths can lead to stability issues as amplitudes increase, the inherently large operating speeds of current EMs are expected to keep pendulum operating amplitudes small. Furthermore, a related open question, is the possibility of exploiting the additional relative pendulum rotational motion inherent in a unifilar architecture to achieve non-circular motion of the pendulum COM, which could enable stability-enhancements and expand the operating and design space of a unifilar CPVA for high-order EM applications.

## 2. DYNAMIC MODEL

In this section, a complete set of governing equations for the unifilar CPVA system are derived using Lagrange's equations, which are linearized and then subsequently used to calculate the system natural frequencies. The unifilar CPVA is shown in Figures 2 - 4. This configuration consists of a pendulum ring of mass  $m_P$  and internal radius b that rolls on a solid roller pin of mass  $m_R$  and radius a. The roller pin rolls within a cut-out of radius b bored into a carrier of inertia  $J_C$ , which is herein referred to as the rotor. The radius of the cut-out in the rotor is required to be the same as the pendulum internal radius. When the cutouts on the rotor and the pendulum are identical it causes the roller to be pinched between two identical surfaces that share the same normal. Specifically, this is between point O and P shown in Figure 3, which are the contact points for the roller and pendulum as well as the roller and rotor, respectively. Due to the centrifugal loading during operation, the roller will maintain contact with the pendulum and the rotor, and is assumed to exhibit pure rolling motion without slip along the two cutout surfaces. If the cutout of the pendulum and rotor are not identical, then the normal forces will not remain diametrically opposed and this can exacerbate the potential of the roller to slip during motion [11].

Figure 2 shows the pendulum at its vertex position, which is its equilibrium position due to the strong centrifugal acceleration imposed by the rotation of the rotor, whose degree of freedom is defined by the angle  $\theta$ . When a torsional disturbance is present on the rotor, the pendulum and roller will begin to oscillate from their equilibrium position and  $R_P(S_P, S_R)$  and  $R_R(S_R)$  defines the radial distance from the center of rotor to the pendulum COM and roller COM, respectively, where  $S_P$  is the arclength displace-

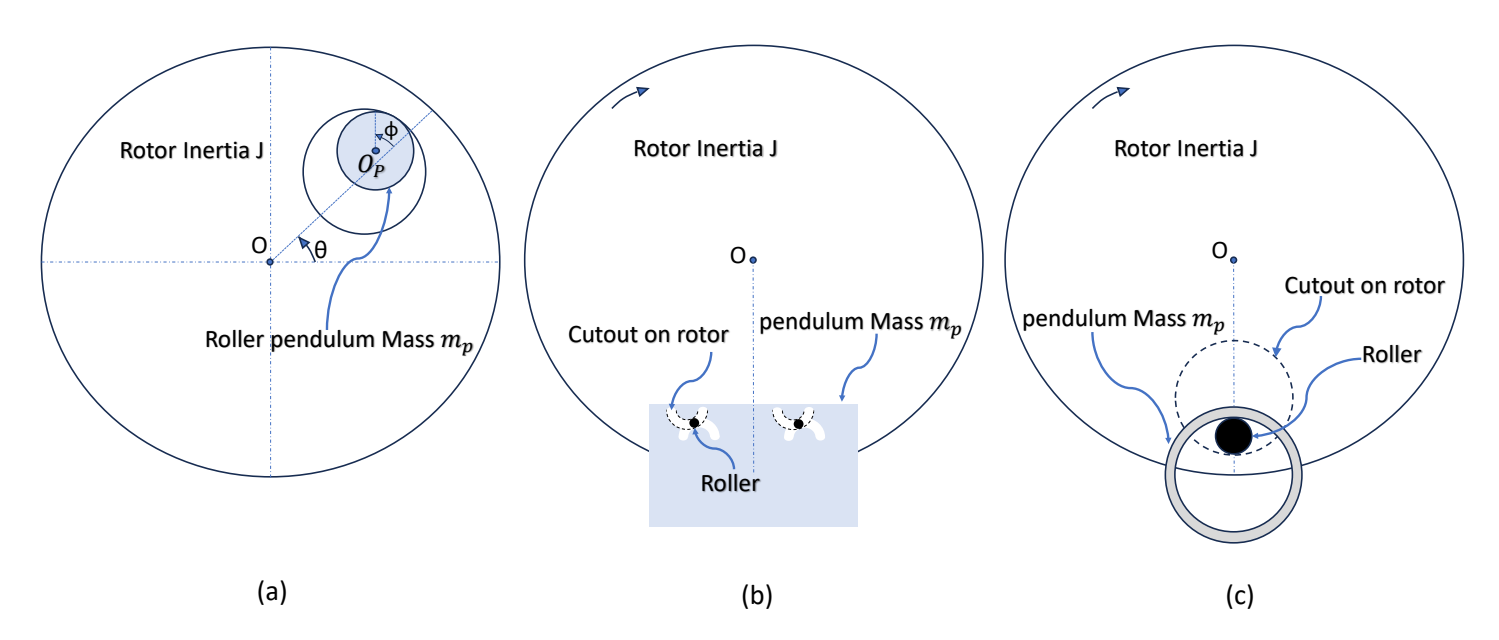


FIGURE 1: Different types of Rotating Vibration Absorbers: (a) Roller-in-slot Type Absorber (b) Bifilar Type Absorber (c) Unifilar Type Absorber [6]

ment of pendulum COM relative to the roller COM and  $S_R$  is the arclength displacement of the roller COM relative to the rotor. Therefore, the three DOFs used herein to describe the configuration of a single unifilar CPVA attached to a rotor include the rotor angle  $\theta$ , the roller arclength displacement  $S_R$ , and the pendulum arclength displacement  $S_P$ . Figures 3 and 4 demonstrate sequentially these three DOFs. Specifically, Figure 3 shows the pendulum and roller when displaced from their vertex position, which is to demonstrate the motion of the absorber system relative to the rotor. It is observed in Figure 3 that the radial distance from center of rotor cutout  $O_C$  to the center of roller  $O_R$  remains the same throughout the motion and hence the path traversed by the roller center is circular with radius  $\rho_0 = b - a$ . In addition, when pendulum and roller share the same tangential velocity at their contact point (and thus move together), then the pendulum center  $O_P$  also follows a circular path trajectory of radius  $2\rho_0 = 2(b-a)$ , relative to point  $O_c$ .

Furthermore, Figure 4 shows the additional rotational motion that the pendulum ring can have relative to the roller pin, which is described by the angle  $\beta$ . This additional DOF of the pendulum results in a double pendulum configuration for the entire system. Specifically, the COM of the roller  $O_R$  and pendulum  $O_P$  can be located relative to the rotor cutout center  $O_C$  using the arclengths  $S_R$  or  $S_P$ , which are related to the angles  $\alpha$  and  $\alpha+\beta$ , respectively. Specifically, for the roller,

$$S_R = \rho_0 \alpha, \tag{1}$$

and for the pendulum,

$$S_P = \rho_0(\alpha + \beta). \tag{2}$$

## 2.1 Kinematics relating pendulum and roller position

Next, we develop kinematic relationships for the unifilar suspension that will be subsequently used in formulating the EOM

for this CPVA system. Specifically, we will derive expressions for the absolute rotations of the roller and pendulum (relative to the rotor) in terms of the arclength DOFs  $S_R$  and  $S_P$ .

To start, as shown Figure 4, we define rotating unit vectors  $\hat{i}$  and  $\hat{j}$ , which rotate with the rotor angular coordinate  $\theta$ . In addition, we define another set of rotating coordinates  $\hat{e}_n$  and  $\hat{e}_t$ , which define the normal and tangent directions associated with the roller center arclength displacements (relative to the rotor motion) and finally we define a set of rotating coordinates  $\hat{e}_\beta$  and  $\hat{e}_p$ , which define the normal and tangent directions associated with the pendulum center arclength displacement (relative to the roller center).

In addition, we define the angle relationships when both the pendulum and roller move together (i.e., when  $S_P=0$ ). As both the roller and pendulum move in unison, the roller and pendulum centers follow the arclength displacement shown in Figure 3, where the roller displacement  $S_R=\rho_0\alpha$  and the pendulum displacement is simply  $2S_R=2\rho_0\alpha$ . During this motion, the roller and pendulum mass rotate with absolute rotation angles  $\phi$  and  $\psi$ , respectively. The tangential velocity of the roller COM  $O_R$  can be expressed in two ways, namely using the local interior angle  $\alpha$  and the absolute roller rotation  $\phi$ , which results in the following velocity constraint

$$(b-a) \dot{\alpha} \hat{e_t} = a \dot{\phi} \hat{e_t}. \tag{3}$$

Similarly, equating the tangential velocities at the pendulum COM  $O_p$  using the interior angle  $\alpha$  and the absolute pendulum rotation  $\psi$ , results in the following kinematic constraint

$$2 (b-a) \dot{\alpha} \hat{e_t} = b \dot{\psi} \hat{e_t}. \tag{4}$$

Eliminating the interior angle  $\alpha$  by combining Equations (3) and (4), enables the pendulum  $\dot{\psi}$  and roller  $\dot{\phi}$ 

angular velocities to be related in the following way

$$\dot{\psi} = \frac{2a}{h}\dot{\phi}.\tag{5}$$

During unison motion, the total rotation of the roller  $\phi$  and pendulum  $\psi$  relative to the rotor can be directly related to the roller arclength position  $S_R$ . Specifically, this is derived by eliminating the angle  $\alpha$  in combining Equations (1) and (3), which results in

$$\phi(S_R) = \frac{S_R}{a},\tag{6}$$

for the roller, and then using this result in Equation (5), which results in

$$\psi(S_R) = \frac{2S_R}{h},\tag{7}$$

for the pendulum.

Similarly, using Equations (1) and (2), the relative rotation of the pendulum  $\beta$  can be expressed in terms of the arclengths  $S_R$  and  $S_P$ , namely

$$\beta = \frac{S_P - S_R}{\rho_0}. (8)$$

Then, the absolute rotation of the pendulum consists of  $\beta(S_R, S_P) - \psi(S_R)$ , which is the superposition of the clockwise defined unison motion as the pendulum rolls with the roller  $\psi(S_R)$  and the counter-clockwise defined relative motion as the pendulum rolls relative to the roller  $\beta(S_R, S_P)$ .

#### 2.2 Equations of motion for the Unifilar CPVA

The dynamic model for the unifilar CPVA system is derived using Lagrange's equations. The kinetic energy of the system *T* consists of the rotational kinetic energy of the rotor as well as both the translational and the rotational kinetic energy of the roller and pendulum, which is expressed as

$$T = \frac{J_C}{2} \vec{\omega}_C \cdot \vec{\omega}_C + \frac{J_R}{2} \vec{\omega}_R \cdot \vec{\omega}_R + \frac{m_R}{2} \vec{v}_R \cdot \vec{v}_R + \frac{J_P}{2} \vec{\omega}_P \cdot \vec{\omega}_P + \frac{m_P}{2} \vec{v}_P \cdot \vec{v}_P,$$
(9)

where  $J_C$  is the inertia of the rotor,  $\vec{\omega}_C = \dot{\theta} \hat{k}$  is the angular velocity of the rotor,  $J_R$  is the inertia of the roller about its COM,  $\vec{\omega}_R$  is the angular velocity of the roller,  $\vec{v}_R$  is the linear velocity of the roller,  $m_R$  is the mass of the roller,  $J_P$  is the inertia of pendulum about its COM,  $\vec{\omega}_P$  is the angular velocity of the pendulum, and  $\vec{v}_P$  is the linear velocity of pendulum, and  $m_P$  is the mass of the pendulum. The total angular velocity of the roller  $\vec{\omega}_R$  includes the rotor rotation rate  $\dot{\theta}$  and the relative roller rotation rate  $\dot{\phi}$  (see Equation (6)),

$$\vec{\omega}_R = (\dot{\theta} - \dot{\phi})\hat{k} = (\dot{\theta} - \dot{S}_R/a)\hat{k}. \tag{10}$$

The total angular velocity of the pendulum  $\vec{\omega}_P$  includes the rotor rotation rate  $\dot{\theta}$  and the total relative pendulum rotation rate  $\dot{\beta} - \dot{\psi}$  (see Equations (7) and (8)),

$$\vec{\omega}_P = (\dot{\theta} - \dot{\psi} + \dot{\beta})\hat{k} = \left(\dot{\theta} + \left(2\frac{a}{b} - 3\right)\dot{S}_R/\rho_0 + \dot{S}_P/\rho_0\right)\hat{k}. \quad (11)$$

Lastly, the roller and pendulum COM velocities  $v_R^2 = \vec{v}_R \cdot \vec{v}_R$  and  $v_P^2 = \vec{v}_P \cdot \vec{v}_P$  can be expressed as

$$\vec{v}_R \cdot \vec{v}_R = \left[ \dot{S}_R \hat{e}_t + \left( \dot{\theta} \hat{k} \times R_R(S_R) \ \hat{e}_{R_R} \right) \right]$$

$$\cdot \left[ \dot{S}_R \hat{e}_t + \left( \dot{\theta} \hat{k} \times R_R(S_R) \ \hat{e}_{R_R} \right) \right]$$

$$= \dot{S}_R^2 + R_R^2 \dot{\theta}^2 + 2 \dot{S}_R \dot{\theta} G_R$$

$$(12)$$

$$\vec{v}_P \cdot \vec{v}_P = \left[ \dot{S}_R \hat{e}_t + \dot{S}_P \hat{e}_\beta + \left( \dot{\theta} \hat{k} \times R_P(S_P, S_R) \ \hat{e}_{R_P} \right) \right]$$

$$\cdot \left[ \dot{S}_R \hat{e}_t + \dot{S}_P \hat{e}_\beta + \left( \dot{\theta} \hat{k} \times R_P(S_P, S_R) \ \hat{e}_{R_P} \right) \right]$$

$$= \dot{S}_P^2 + \dot{S}_R^2 + R_P^2 \dot{\theta}^2 + 2 \dot{S}_P \dot{\theta} G_P$$

$$+ \dot{S}_R \dot{\theta} \left( 2G_P \cos \left( \frac{S_P - S_R}{\rho_0} \right) - \frac{dR_P^2}{dS_P} \sin \left( \frac{S_P - S_R}{\rho_0} \right) \right),$$

$$(13)$$

where  $\hat{e}_{R_R}$  and  $\hat{e}_{R_P}$  are radial unit vectors whose directions specify the rollers radial position  $R_R(S_R)$  and the pendulums radial position  $R_P(S_R, S_P)$  relative to the rotor center, respectively. The path functions  $G_R$  and  $G_P$  result from the vector cross and dot product and can be expressed in terms of the roller and pendulum radial positions, specifically

$$G_R(S_R) = \sqrt{R_R^2(S_R) - \frac{1}{4} \left(\frac{\partial R_R^2(S_R)}{\partial S_R}\right)^2},$$
 (14)

and

$$G_P(S_P, S_R) = \sqrt{R_P^2(S_P, S_R) - \frac{1}{4} \left( \frac{\partial R_P^2(S_P, S_R)}{\partial S_P} \right)^2}.$$
 (15)

The Lagrangian  $\mathcal{L} = T - V$  of the system is expressed as follows

$$\frac{d}{dt} \left( \frac{\partial \mathcal{L}}{\partial \dot{q}_i} \right) - \frac{\partial \mathcal{L}}{\partial q_i} = Q_i, \tag{16}$$

where T is the system kinetic energy, V is the system potential energy,  $q_i$  is the generalized coordinates, which includes the roller position  $S_R$ , the pendulum position  $S_P$ , and the rotor rotation angle  $\theta$ , and  $Q_i$  corresponds to the generalized forces acting on the system. Here we set  $Q_i = 0$  since our interest is in deriving the natural frequencies of this system. Since the centrifugal forces are many orders of magnitude greater than the gravitational forces, the potential energy is commonly ignored in modeling a CPVA system and therefore the Lagrangian  $\mathcal{L} = T$ . Using Equation (16), the EOM for pendulum motion  $S_P$  is

$$(1 + \kappa_P) \ddot{S}_P + \left[\cos\left(\frac{S_P - S_R}{\rho_0}\right) + \kappa_P(2\chi - 3)\right] \ddot{S}_R + \left(\dot{S}_R^2/\rho_0 + 2\dot{S}_R\dot{\theta}\right) \sin\left(\frac{S_P - S_R}{\rho_0}\right) + \rho_0 \ddot{\theta} \left[(\tilde{n}_0^2 - 1)\cos(S_P/\rho_0) + \kappa_P + 1 + \cos\left(\frac{S_P - S_R}{\rho_0}\right)\right] + \rho_0 \dot{\theta}^2 \left[(\tilde{n}_0^2 - 1)\sin(S_P/\rho_0) + \sin\left(\frac{S_P - S_R}{\rho_0}\right)\right] = 0 \quad (17)$$

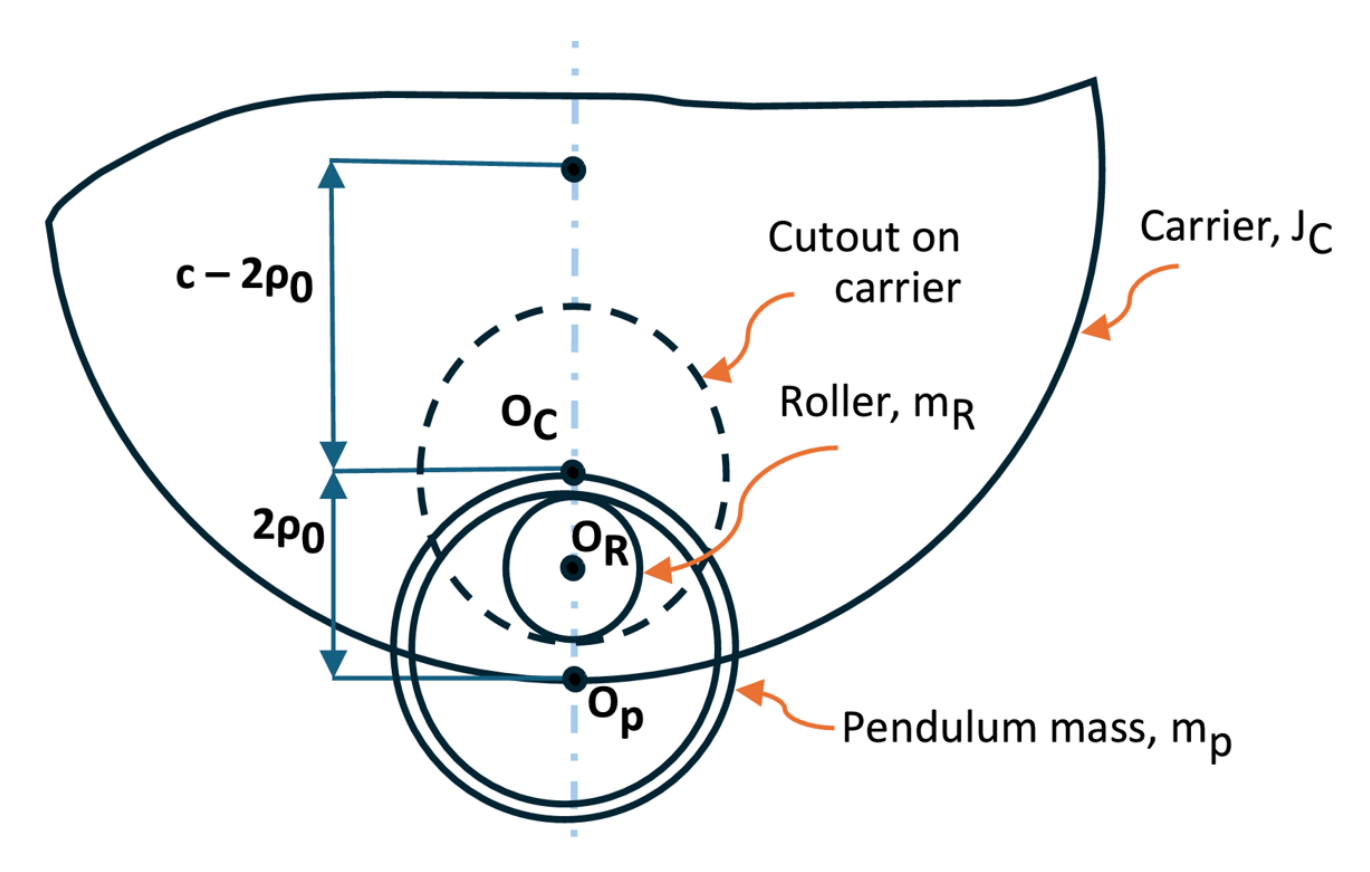


FIGURE 2: Schematic view of a Unifilar CPVA assembly on the carrier at its equilibrium position.

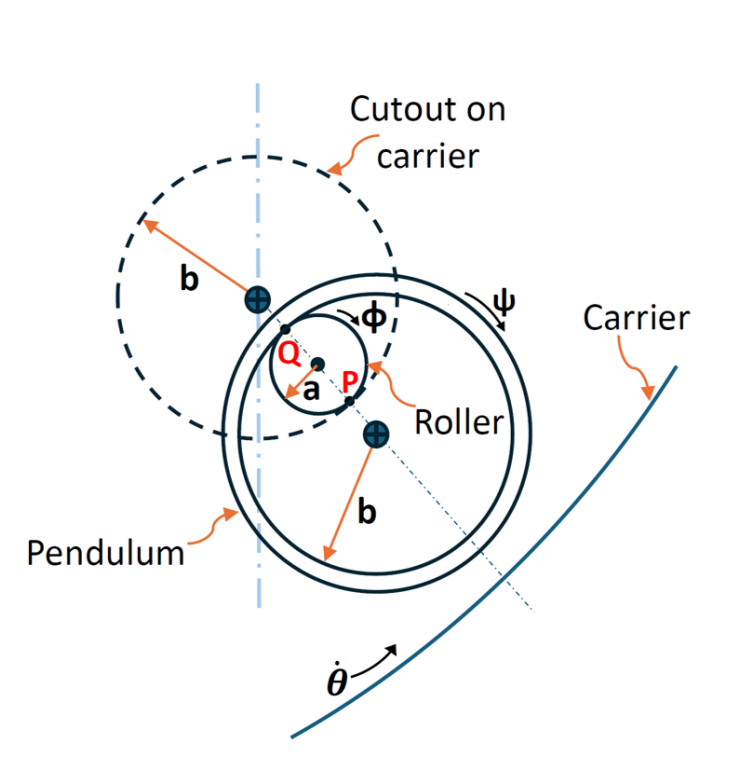


FIGURE 3: Off-vertex position of the Unifilar CPVA when both the roller and pendulum roll in unison.

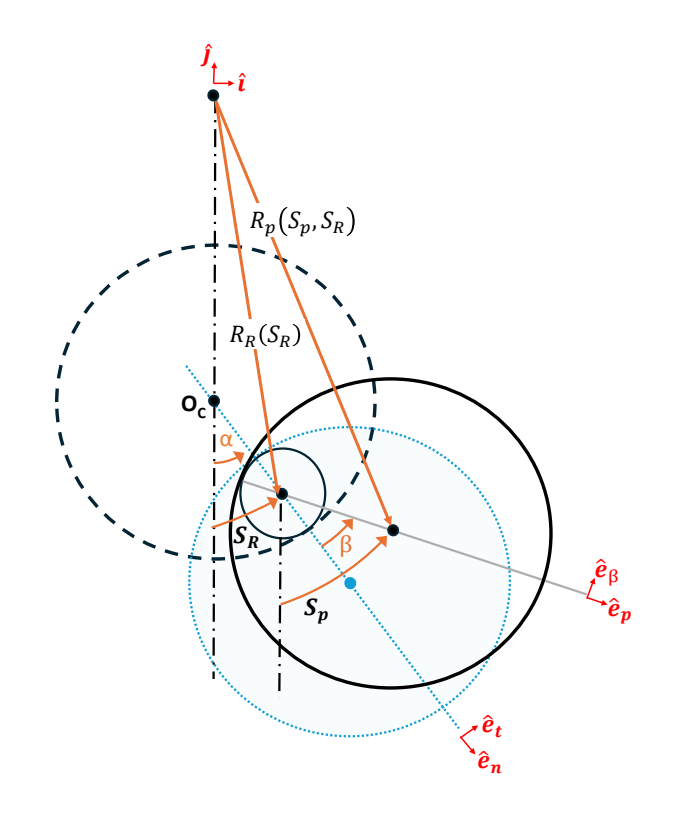


FIGURE 4: Off-vertex position of the Unifilar CPVA when the pendulum rotates with the additional angle  $\beta$  relative to its unison motion with the roller pin.

where  $\kappa_P = (k_P/\rho_0)^2$  and  $\chi = a/b$  are non-dimensional terms related to the pendulum radius of gyration  $k_P$  and the roller and pendulum geometries a, b, and  $\rho_0 = b - a$ . In addition,  $\tilde{n}_0$  is the well-known classical absorber linear tuning order for a single pendulum absorber mass [12], which for the case of a point mass is dictated solely by the absorbers geometry, that is

$$\tilde{n}_0 = \sqrt{\frac{c - \rho_0}{\rho_0}},\tag{18}$$

where  $c - \rho_0$  is the distance from the pendulum mass pivot point to the rotor center and  $\rho_0$  is the effective pendulum length, which is distance from the pivot point to the center of mass of pendulum. As shown in Figure 2 and 4, the pendulum pivot point is the roller center, point  $O_R$ . Note that we have also substituted the radial positions of the roller  $R_R(S_R)$  and the pendulum  $R_P(S_P, S_R)$  into the Lagrangian before computing the EOM (See Appendix A for further details). Similarly, the EOM for the roller motion  $S_R$  is

$$\left[1 + \epsilon \left(1 + \kappa_R (1/\chi - 1)^2\right) + \kappa_P \left(9 + 4\chi^2 - 12\chi\right)\right] \ddot{S}_R + \left[\cos\left(\frac{S_P - S_R}{\rho_0}\right) + \kappa_P (2\chi - 3)\right] \ddot{S}_P + \rho_0 \ddot{\theta} \left[(1 + \epsilon)\left(1 + (\tilde{n}_0^2 - 1)\cos(S_R/\rho_0)\right) + \cos\left(\frac{S_P - S_R}{\rho_0}\right) + \kappa_P (2\chi - 3) - \kappa_R (1/\chi - 1)\right] - \sin\left(\frac{S_P - S_R}{\rho_0}\right) \left[\dot{S}_P^2/\rho_0 + 2\dot{S}_P \dot{\theta}\right] + \rho_0 \dot{\theta}^2 \left[(1 + \epsilon)(\tilde{n}_0^2 - 1)\sin(S_R/\rho_0) - \sin\left(\frac{S_P - S_R}{\rho_0}\right)\right] = 0, \quad (19)$$

where  $\kappa_R = (k_R/\rho_0)^2$  is the ratio of the roller radius of gyration  $k_R$  to the effective pendulum length  $\rho_0$ . Finally, the EOM for the rotor motion  $\theta$  is

$$\begin{split} \left[\gamma + \kappa_P + \kappa_R + \epsilon \left(1 + (\tilde{n}_0^2 - 1)^2\right) + 2\left(1 + (\tilde{n}_0^2 - 1)\cos\left(\frac{S_P}{\rho_0}\right)\right) + \\ 2(\tilde{n}_0^2 - 1)\cos\left(\frac{S_R}{\rho_0}\right)(1 + \epsilon) + 2\cos\left(\frac{S_P - S_R}{\rho_0}\right)\right]\rho_0\ddot{\theta} + \\ \left[1 + \kappa_P + (\tilde{n}_0^2 - 1)\cos\left(\frac{S_P}{\rho_0}\right) + \cos\left(\frac{S_P - S_R}{\rho_0}\right)\right]\ddot{S}_P + \\ \left[1 - \kappa_R(1/\chi - 1) + (\tilde{n}^2 - 1)\cos\left(\frac{S_R}{\rho_0}\right)(1 + \epsilon) + (2\chi - 3)\kappa_P + \\ \cos\left(\frac{S_P - S_R}{\rho_0}\right) + \epsilon\right]\ddot{S}_R + \left[\left(-(\tilde{n}^2 - 1)\sin\left(\frac{S_P}{\rho_0}\right) - \sin\left(\frac{S_P - S_R}{\rho_0}\right)\right)\right] \\ \left(2\dot{S}_P\dot{\theta} + \frac{\dot{S}_P^2}{\rho_0}\right) + \left[(\tilde{n}^2 - 1)\sin\left(\frac{S_R}{\rho_0}\right)(-1 - \epsilon) + \left(\frac{S_P - S_R}{\rho_0}\right)\right] \\ \left(2\dot{\theta}\dot{S}_R + \frac{\dot{S}_R^2}{\rho_0}\right) = 0 \quad (20) \end{split}$$

where  $\gamma = J_C/(m_P \rho_0^2)$  is the ratio of rotor inertia to pendulum inertia (about its pivot point  $O_R$ ).

## 2.3 Linear tuning order of a unifilar CPVA

Next, we linearize the EOM to identify the small amplitude natural frequency of the CPVA system, which provides insight into how the roller and pendulum mass, inertia, and geometry affect the tuning of this system. To linearize the EOM, we assume small amplitude motions for  $S_R$  and  $S_P$ , and that the rotor rotates with constant angular velocity  $\dot{\theta} = \Omega$  and therefore  $\ddot{\theta} = 0$ .

The linear EOM for the pendulum motion  $S_P$  is

$$(1 + \kappa_P)\ddot{S}_P + \left[1 + \kappa_P(2\chi - 3)\right]\ddot{S}_R + (\tilde{n}_0\Omega)^2 S_P - \Omega^2 S_R = 0.$$
 (21)

The linear EOM for the roller motion  $S_R$  is

$$\begin{split} & \left[ 1 + \epsilon \left( 1 + \kappa_R (1/\chi - 1)^2 \right) + \kappa_P (9 + 4\chi^2 - 12\chi) \right] \ddot{S}_R + \\ & + \left[ 1 + \kappa_P (2\chi - 3) \right] \ddot{S}_P + \left( \tilde{n}_0^2 (1 + \epsilon) - \epsilon \right) \Omega^2 S_R - \Omega^2 S_P = 0. \end{split} \tag{22}$$

The coupled set of a linear EOM for the system can be cast in a matrix form,

$$\mathbf{M}\ddot{\vec{S}} + \mathbf{K}\vec{S} = 0, \tag{23}$$

where  $\vec{S} = [S_P, S_R]^T$ , the system mass matrix **M** is

M =

$$\begin{bmatrix} 1 + \kappa_P & 1 + \kappa_P (2\chi - 3) \\ 1 + \kappa_P (2\chi - 3) & 1 + \epsilon \left( 1 + \kappa_R \left( \frac{1}{\chi} - 1 \right)^2 \right) + \kappa_P (9 + 4\chi^2 - 12\chi) \end{bmatrix},$$
(24)

and the system stiffness matrix K is

$$\mathbf{K} = \Omega^2 \begin{bmatrix} \tilde{n}_0^2 & -1 \\ -1 & \tilde{n}_0^2 (1 + \epsilon) - \epsilon \end{bmatrix}, \tag{25}$$

Next, we solve the eigenvalue problem to obtain the two system natural frequencies  $\omega_1$  and  $\omega_2$ , specifically by computing the following determinant

$$|\mathbf{K} - \omega_i^2 \mathbf{M}| = 0, \tag{26}$$

whose roots (the natural frequencies) are proportional to the linear tuning orders of the system  $\tilde{n}_1$  and  $\tilde{n}_2$ , where  $\omega_1 = \tilde{n}_1 \Omega$  and  $\omega_2 = \tilde{n}_2 \Omega$ . It can be observed that the rotor speed  $\Omega^2$  can be prefactored in Equation (26), and the resulting determinant yields the following quadratic equation for the system tuning orders  $\tilde{n}_1$  and  $\tilde{n}_2$ ,

$$\left[4\kappa_{P}(\chi-2)^{2} + \epsilon(1+\kappa_{P})\chi^{-2}(\kappa_{R}(\chi-1)^{2} + \chi^{2})\right]\tilde{N}^{2} + \left[\epsilon\left(1-2\tilde{n}_{0}^{2} + \kappa_{P}(1+\tilde{n}_{0}^{2}) - \kappa_{R}\chi^{-2}\tilde{n}_{0}^{2}(\chi-1)^{2}\right) - 2\left(1+\tilde{n}_{0}^{2} + \kappa_{P}\left(2\chi - 3 + \tilde{n}_{0}^{2}(5+2\chi(\chi-3))\right)\right)\right]\tilde{N} + (\tilde{n}_{0}^{2} - 1)\left(\tilde{n}_{0}^{2}(1+\epsilon) + 1\right) = 0, \tag{27}$$

where the two roots  $\tilde{N}_{1,2}$  of Equation (27) are related to the two system tuning orders,  $\tilde{n}_1 = \sqrt{\tilde{N}_1}$  and  $\tilde{n}_2 = \sqrt{\tilde{N}_2}$ .

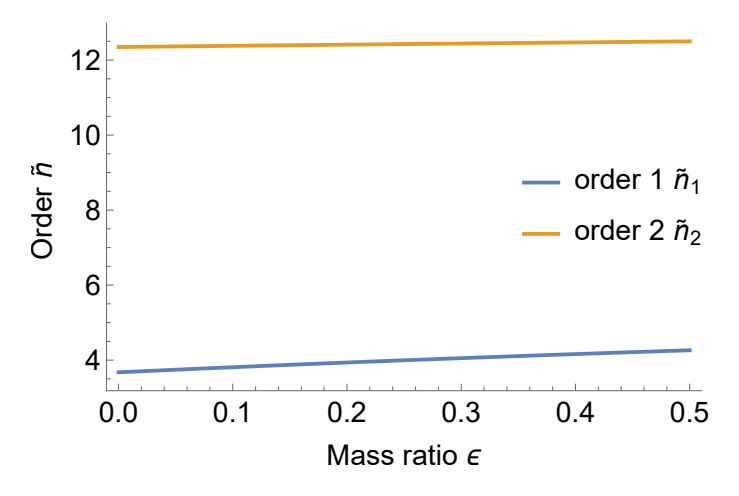


FIGURE 5: Tuning order versus mass ratio of both pendulums. Parameters:  $\kappa_P=4,\,\kappa_R=0.25,\,a=0.183$  mm, b=0.366 mm and  $\chi=0.5.$ 

Figure 5 shows the effect of roller to pendulum mass ratio  $\epsilon$ on the tuning orders  $\tilde{n}_1$  and  $\tilde{n}_2$  for a prototype 12th order design, which is a possible order of excitation for an EM. In this design, we consider a pendulum radius "b = 2a" that is twice the roller radius "a", which aligns with the concept of a comparatively larger pendulum and a smaller roller. The tuning order corresponding to  $\tilde{n}_2$  is the primary resonance that will address a problematic torsional vibration at order 12 and we have slightly overtuned this resonance by about 3% (relative to 12), which is common practice in circular path design (see for example [13]). The other tuning order  $\tilde{n}_1$  is a result of the double pendulum architecture. As shown in Figure 5, the roller to pendulum mass ratio  $\epsilon$  does influence both tuning orders, however, the primary resonance  $\tilde{n}_2$  is rather insensitive to this as it varies by less than 1% over the range of  $\epsilon$  shown. Whereas, the secondary resonance  $\tilde{n}_1$  shows about a 10% variation over this range of  $\epsilon$ . This redundant order  $\tilde{n}_1$  does present challenges when tuning to a single order of excitation. However, for the small roller and large pendulum design, it does shows a desirable large separation, where  $\tilde{n}_1$  is about 3 times less than the primary tuning order  $\tilde{n}_2$ .

Furthermore, Figure 6 shows the influence of the radius of gyration of the pendulum on the tuning order for a fixed mass ratio  $\epsilon = 0.10$ . The pendulum inner radius "b = 2a" is still twice that of the roller radius "a", but we now consider increasing the outer radius of the pendulum ring, which will increase the radius of gyration of the pendulum. In this case, we allow the pendulum outer radius to increase from 2a to 4a, which would increase the non-dimensional radius of gyration parameter  $\kappa_P$ from 4 to 10. In further support of the large pendulum and small roller design, Figure 6 favorably shows that increasing the pendulum ring thickness can further separate the two orders, with the primary order  $\tilde{n}_2$  being negligibly affected. We believe the large separation should make this design feasible to implement, minimizing the possibility of rotor disturbance at the redundant order  $\tilde{n}_1$ . Future simulation work of the forced response will further investigate this.

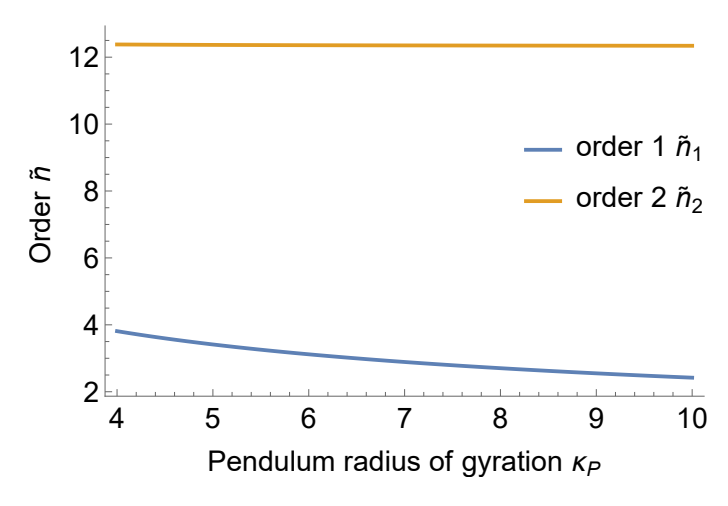


FIGURE 6: Tuning order versus pendulum radius of gyration. Parameters:  $\kappa_R=0.25,~a=0.183$  mm, b=0.366 mm,  $\chi=0.50$ , and  $\epsilon=0.1$ 

#### 3. CONCLUSION

In this paper, a unifilar CPVA architecture is specifically proposed for electrified motor applications that consists of a large outer pendulum ring suspended from a small roller pin. A qualitative comparison is made between the unifilar, bifilar and roller-inslot configurations. A unifilar-type absorber has inherent advantages in terms of its simple mechanical construction compared to that of the bifilar when considering the machining challenges associated with non-circular path design and the high-orders present in current EMs. A unifilar also has an advantage over the roller-in-slot design, in that the roller is diametrically pinched between the pendulum and rotor, which reduces the propensity of the roller to slip and thus avoiding problematic dynamic responses of the CPVA and rotor.

A dynamic model for a unifilar CPVA is developed and then linearized to compute the tuning orders of the system. Compared to the bifilar and roller-in-slot designs, the unifilar is a double pendulum architecture and this results in two tuning orders for the system. A quadratic formula is derived whose roots govern the two natural orders of the system and initial results show a desirable large separation between these orders in a prototype 12th order CPVA design. Although circular paths can lead to stability issues as amplitudes increase, the inherently large operating speeds of current EMs are expected to keep pendulum operating amplitudes small. High excitation still poses instability risks however, and hence standard over-tuning to keep amplitudes low may be required (see for example [13]). Furthermore, a related open question, is the possibility of exploiting the additional relative pendulum rotational motion inherent in a unifilar architecture to achieve non-circular motion of the pendulum COM, which could enable stability-enhancements and expand the operating and design space of a unifilar CPVA for high-order EM applications. The developed model will facilitate these future simulation and analysis studies of the system forced vibration response to characterize the stability and vibration control performance of this design.

#### **REFERENCES**

- [1] "Key aspects of the Paris Agreement." Accessed may 29, 2024, URL https://unfccc.int/most-requested/key-aspects-of-the-paris-agreement#: ~:text=The%20Paris%20Agreement's%20central%20aim, further%20to%201.5%20degrees%20Celsius.
- [2] Bilgin, Berker and Emadi, Ali. "Electric Motors in Electrified Transportation: A step toward achieving a sustainable and highly efficient transportation system." *IEEE Power Electronics Magazine* Vol. 1 No. 2 (2014): pp. 10–17. DOI 10.1109/MPEL.2014.2312275.
- [3] "ZF Intelligently Designs New Generation 8-speed Automatic Transmission for Hybrid Drives." (2019). Accessed May 24, 2024, URL https://press.zf.com/press/en/releases/release\_9857.html.
- [4] Wu, Guangqiang and Zhang, Yi. "A review of research on centrifugal pendulum vibration absorber in the field of vehicle power transmission." *Proceedings of the Institution of Mechanical Engineers, Part D: Journal of Automobile Engineering* (2023)DOI 10.1177/09544070231194743.
- [5] "Design and Tuning of Centrifugal Pendulum Vibration Absorbers for Nonlinear Response." 2017. URL https://api.semanticscholar.org/CorpusID:117346159.
- [6] Wilson, W Ker. "Practical solution of torsional vibration problems: with examples from marine, electrical, aeronautical and automobile engineering practice." (No Title) (1956).
- [7] Shaw, Steven and Geist, Bruce. "Tuning for Performance and Stability in Systems of Nearly Tautochronic Torsional Vibration Absorbers." *Journal of Vibration and Acoustics* Vol. 132 (2010). DOI 10.1115/1.4000840.
- [8] Duh, James E. and Miao, Wu. "Development of monofilar rotor hub vibration absorber." 1983. URL https://api.semanticscholar.org/CorpusID:118552776.
- [9] Manchi, Venkateswararao and Sujatha, C. "Torsional vibration reduction of rotating shafts for multiple orders using centrifugal double pendulum vibration absorber." Applied Acoustics (2020): p. 107768URL https://api.semanticscholar.org/CorpusID:230605535.
- [10] Mahe, Vincent. "Improvements in the design of pendulum absorbers to reduce the vibrations of automotive powertrains." Theses, HESAM Université. 2022. URL https://pastel.hal.science/tel-04058834.
- [11] Geist, Bruce, Ramakrishnan, Venkatanarayanan, Attibele, Pradeep and Resh, William. "Precision requirements for the bifilar hinge slots of a centrifugal pendulum vibration absorber." *Precision Engineering* Vol. 52 (2018): pp. 1– 14. URL http://dx.doi.org/10.1016/j.precisioneng.2017.08. 001.
- [12] Denman, HH. "Tautochronic bifilar pendulum torsion absorbers for reciprocating engines." *Journal of Sound and*

- *Vibration* Vol. 159 No. 2 (1992): pp. 251–277. URL https://api.semanticscholar.org/CorpusID:121289979.
- [13] Newland, D. E. "Nonlinear Aspects of the Performance of Centrifugal Pendulum Vibration Absorbers." *ASME Journal of Engineering for Industry* (1964): pp. 257–263DOI 10.1115/1.3670529.

### 4. APPENDIX A

Parametric equations for the radial positions of the COM of the roller  $R_R(S_R)$  as well as the pendulum  $R_P(S_P, S_R)$  are derived here in terms of arclength parameters  $S_P$  and  $S_R$ . Specifically, the horizontal position  $X_P$  and vertical position  $Y_P$  of the pendulum COM relative to a rotor fixed coordinate system  $(\hat{i}, \hat{j})$  (see Figure 4) can be expressed as,

$$X_{P} = \rho_{0} \sin \alpha + \rho_{0} \sin (\alpha + \beta),$$

$$= \rho_{0} \sin \left(\frac{S_{R}}{\rho_{0}}\right) + \rho_{0} \sin \left(\frac{S_{P}}{\rho_{0}}\right)$$
(28)

$$Y_{P} = (c - 2\rho_{0}) + \rho_{0} \cos \alpha + \rho_{0} \cos (\alpha + \beta),$$

$$= (c - 2\rho_{0}) + \rho_{0} \cos \left(\frac{S_{R}}{\rho_{0}}\right) + \rho_{0} \cos \left(\frac{S_{P}}{\rho_{0}}\right). \quad (29)$$

Similarly, the horizontal  $X_R$  and vertical  $Y_R$  position of the roller COM relative to a rotor fixed coordinate system  $(\hat{i}, \hat{j})$  (see Figure 4) can be expressed as,

$$X_R = \rho_0 \sin \alpha,$$

$$= \rho_0 \sin \left(\frac{S_R}{\rho_0}\right)$$
(30)

$$Y_R = (c - 2\rho_0) + \rho_0 \cos \alpha,$$
  
=  $(c - 2\rho_0) + \rho_0 \cos \left(\frac{S_R}{\rho_0}\right),$  (31)

where we make use of Equations (1) and (2) to replace  $\alpha$  and  $\beta$  and express these positions in terms of the arclengths  $S_R$  and  $S_P$ . Finally, the pendulum radial position  $R_p^2 = X_p^2 + Y_p^2$  can be calculated using Equations (28) and (29), which results in,

$$\begin{split} R_p^2(S_P, S_R) &= c^2 - 4c\rho_0 + 2\rho_0^2 \left[ 3 + \cos\left(\frac{S_P - S_R}{\rho_0}\right) \right] \\ &+ 2(c - 2\rho_0)\rho_0 \left[ \cos\left(\frac{S_P}{\rho_0}\right) + \cos\left(\frac{S_R}{\rho_0}\right) \right] \end{split}$$

Likewise, the roller radial position  $R_R^2 = X_R^2 + Y_R^2$  can be calculated from Equations (30) and (31), which results in,

$$R_R^2(S_R) = c^2 + 5\rho_0^2 - 4c\rho_0 + 2(c - 2\rho_0)\rho_0 \cos\left(\frac{S_R}{\rho_0}\right)$$
 (32)